J Mol Model (2012) 18:307–318
DOI 10.1007/s00894-011-1057-9

ORIGINAL PAPER

Noscapinoids with anti-cancer activity against human acute lymphoblastic leukemia cells (CEM): a three dimensional chemical space pharmacophore modeling and electronic feature analysis

Pradeep K. Naik · Seneha Santoshi · Harish C. Joshi

Received: 1 January 2011 / Accepted: 22 March 2011 / Published online: 27 April 2011

Abstract We have identified a new class of microtubule-binding compounds—noscapinoids—that alter microtubule dynamics at stoichiometric concentrations without affecting tubulin polymer mass. Noscapinoids show great promise as chemotherapeutic agents for the treatment of human cancers. To investigate the structural determinants of noscapinoids responsible for anti-cancer activity, we tested 36 structurally diverse noscapinoids in human acute lymphoblastic leukemia cells (CEM). The IC_{50} values of these noscapinoids vary from 1.2 to 56.0 μM. Pharmacophore models of anti-cancer activity were generated that identify two hydrogen bond acceptors, two aromatic rings, two hydrophobic groups, and one positively charged group as essential structural features. Additionally, an atom-based quantitative structure–activity relationship (QSAR) model was developed that gave a statistically satisfying result (R^2=0.912, Q^2=0.908, Pearson R=0.951) and effectively predicts the anti-cancer activity of training and test set compounds. The pharmacophore model presented here is well supported by electronic property analysis using density functional theory at B3LYP/3-21*G level. Molecular electrostatic potential, particularly localization of negative potential near oxygen atoms of the dimethoxy isobenzofuranone ring of active compounds, matched the hydrogen bond acceptor feature of the generated pharmacophore. Our results further reveal that all active compounds have smaller lowest unoccupied molecular orbital (LUMO) energies concentrated over the dimethoxy isobenzofuranone ring, azido group, and nitro group, which is indicative of the electron acceptor capacity of the compounds. Results obtained from this study will be useful in the efficient design and development of more active noscapinoids.

Keywords Noscapinoid · Pharmacophore · 3D QSAR · Electrostatic potential profile · Lowest unoccupied molecular orbital · Highest occupied molecular orbital · Free energy of solvation

P. K. Naik (✉) · H. C. Joshi (✉)
Department of Cell Biology,
Emory University School of Medicine,
615 Michael Street,
Atlanta, GA 30322, USA
e-mail: pnaik2@emory.edu

H. C. Joshi
e-mail: joshi@cellbio.emory.edu

S. Santoshi
Department of Biotechnology and Bioinformatics,
Jaypee University of Information Technology,
Waknaghat, Solan 173215 Himachal Pradesh, India

Introduction

Phthalideisoquinoline [(S)-3-((R)-4-methoxy-6-methyl-5,6,7,8-tetrahydro-[1,3]dioxolo[4,5-g]isoquinolin-5-yl)-6,7-dimethoxyiso-benzofuran-1(3 H)-one], also commonly known as noscapine (Fig. 1), is a plant-derived non-toxic orally available alkaloid that has been used clinically as a cough suppressant in humans and in experimental animals [1–3]. Its role as a stoichiometric tubulin-binding anti-cancer drug was discovered in our laboratory [4]. Noscapine binds to tubulin and alters tubulin conformation as determined by significant changes in the circular dichroism spectra of tubulin [4]. Unlike other clinically used microtubule(MT)-binding drugs such as vincas (MT

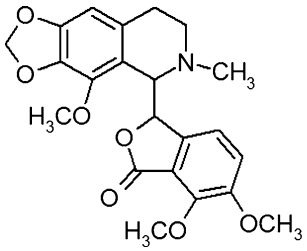

Fig. 1 Chemical structure of noscapine, which consists of an isoquinoline ring (*top section*) and a dimethoxy isobenzofuranone ring (*lower section*)

depolymerizing) and taxanes (MT over-polymerizing and bundling), noscapine simply suppresses the dynamics of MT assembly without changing the dimer/polymer ratio, blocks mitotic progression, and induce apoptosis in many cancer cell types [4–7]. Our laboratory has now synthesized more potent noscapine derivatives (collectively called noscapinoids) that may be suited for development of yet better anti-cancer agents [8–13]. This array of compounds led us to evaluate quantitatively the structure–activity relationships of noscapinoids.

In this study, we evaluate the structure–activity relationship of noscapinoids by developing pharmacophore models. The quality of pharmacophores was examined by atom-based 3D quantitative structure-activity relationship (QSAR) models [14] using Pharmacophore Alignment and Scoring Engine (PHASE, Schrodinger suite). This engine has been used successfully in many drug discovery studies such as those investigating glycoprotein (GP)IIb/IIIa antagonists [15], H3-antihistaminics [16], MRP1 modulators [17], and dihydrofolate reductase inhibitors [18]. Additionally, we performed several quantum chemical calculations to analyze the role of the calculated electronic properties in identifying a pharmacophore model for anti-cancer activity. Electronic features are particularly helpful, not only in the design of new drugs and in helping to understand their mechanism of action [19–24] but also in predicting potential reactive sites that may lead to off-target effects. Electronic properties such as molecular electrostatic profile (MESP), lowest unoccupied molecular orbital (LUMO), highest occupied molecular orbital (HOMO), and aqueous solvation energy are very useful parameters for an accurate understanding of the chemical reactivity of molecules [19–21, 25]. MESP is a widely used and proven tool for exploring molecular electronic structure, reactivity patterns, and structure–activity relationship studies [22–24].

We believe that our ligand-based approaches to identifying pharmacophore models will provide important insights that will lead to the design of novel noscapinoids as anti-cancer agents. Furthermore, determination of the molecular electronic properties responsible for the potent anti-cancer activity of noscapine and its congeners should pinpoint the fundamental molecular-level forces responsible for their potency.

Materials and methods

Biological data

We used 36 noscapine derivatives (noscapinoids) that were synthesized in our laboratory [8–13] for pharmacophore generation (Table 1). Structural modifications were introduced primarily in the isoquinoline and benzyl furanone rings of noscapine (Fig. 1). Anti-cancer activities of these compounds were measured against CEM, a multi-drug resistant human T-cell lymphoblastoid cell line under identical experimental conditions (to minimize bias). A drug-resistant CEM cell line (overexpressing the drug efflux pumps, MDR and MRP [26]) was generously provided by W.T. Beck (Cancer Center, University of Illinois at Chicago). Cell culture reagents were obtained from Mediatech (http://cellgro.com). Cells were grown in RPMI 1640 medium (Mediatech) supplemented with 10% fetal calf serum, 1% antibiotics (penicillin/streptomycin), 2 mM 1-glutamine, at 37°C in a humidified atmosphere with 5% CO_2. Cell proliferation assay was performed in 96-well plates as previously described [9, 27]. Briefly, cells were seeded in 100 μL growth medium at a density of 5 x 10^3 cells per well in 96-well plates and allowed to establish for 24 h. Serially diluted concentrations (0.01–500 μM) of noscapinoids were then added and cells were incubated for 72 h. We measured the inhibition of cell proliferation in a colorimeter by 3-(4,5-dimethylthiazol-2-yl)-5-(3-carboxymethoxyphenyl)-2-(4-sulfophenyl)-2 H-tetrazolium inner salt (MTS) assay using the CellTiter96 AQ_{ueous} One Solution Reagent (Promega, Madison, WI). Cells were incubated with MTS for 3 h and absorbance was measured at a wavelength of 490 nm using a microplate reader (Molecular Devices, Sunnyvale, CA). The percentage of cell survival as a function of drug concentration was then plotted to determine the IC_{50} values (the drug concentration needed to prevent cell proliferation by 50%). The negative logarithm of the measured IC_{50} value in molar concentration (expressed as pIC_{50} values) of these compounds was used in the pharmacophore modeling and QSAR study.

Generation of the common pharmacophore hypotheses

In order to rationalize chemical structure with the observed anti-cancer activity, pharmacophore models were developed using a dataset of 36 noscapinoids. Molecular models of these structures were built using the builder panel in Maestro (version 9.1; Schrodinger package, [28]). Each structure was assigned an appropriate bond order using ligprep script [28] and was subsequently subjected to energy minimization using the OPLS 2005 force field with a dielectric constant of 1.0. In the development of common pharmacophore hypotheses (CPHs) for anti-cancer activity

Table 1 Chemical structures of noscapine and its congeners used in the present study, along with their observed inhibitory activity of cell proliferation (CEM cell line)

Sl No.	Compound Structure	IC_{50} (M)	Sl No.	Compound Structure	IC_{50} (M)
1	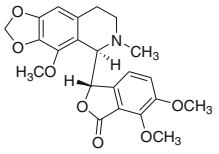	16.59×10^{-6}	2	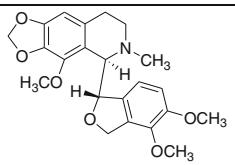	28.3×10^{-6}
3	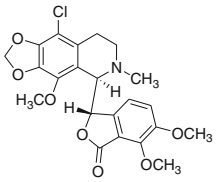	1.2×10^{-6}	4	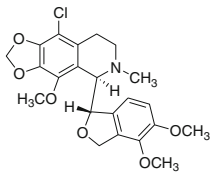	45.2×10^{-6}
5	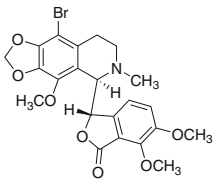	1.9×10^{-6}	6	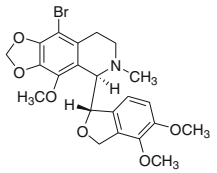	2.8×10^{-6}
7	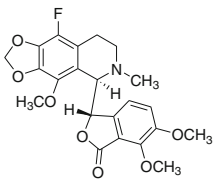	2.3×10^{-6}	8	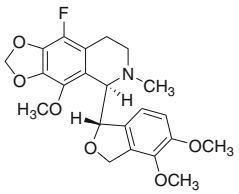	15.5×10^{-6}
9	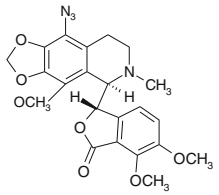	2.6×10^{-6}	10	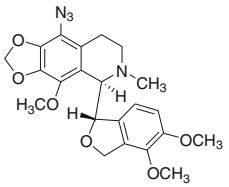	2.6×10^{-6}
11	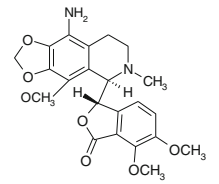	3.0×10^{-6}	12	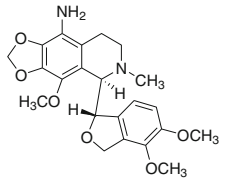	3.0×10^{-6}
13	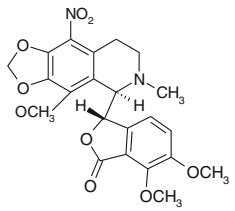	10.0×10^{-6}	14	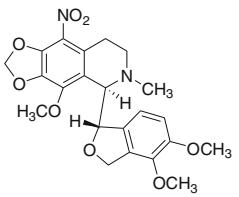	10.0×10^{-6}
15	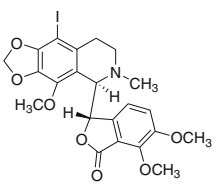	38.9×10^{-6}	16	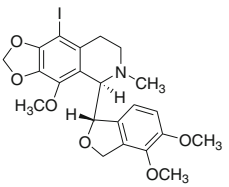	30.5×10^{-6}

Table 1 (continued)

#	Compound Structure	IC_{50} (M)	#	Compound Structure	IC_{50} (M)
17	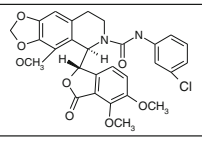	48.0×10^{-6}	18	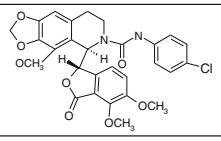	45.2×10^{-6}
19	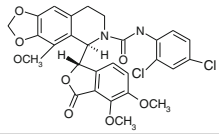	44.2×10^{-6}	20	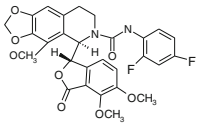	40.6×10^{-6}
21	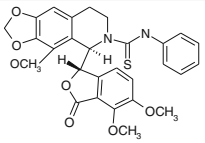	41.9×10^{-6}	22	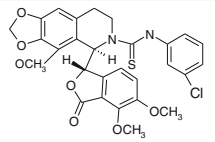	45.1×10^{-6}
23	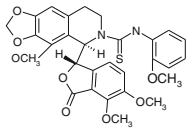	46.5×10^{-6}	24	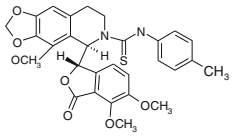	44.4×10^{-6}
25	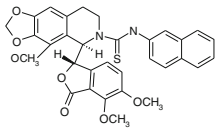	44.1×10^{-6}	26	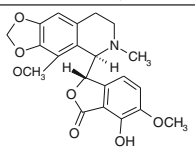	51.8×10^{-6}
27	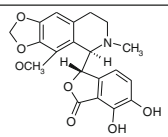	39.5×10^{-6}	28	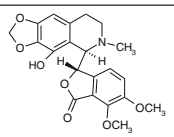	42.6×10^{-6}
29	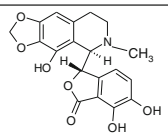	41.0×10^{-6}	30	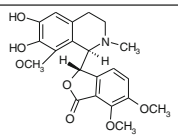	42.3×10^{-6}
31	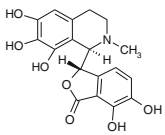	35.5×10^{-6}	32	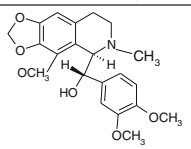	53.6×10^{-6}
33	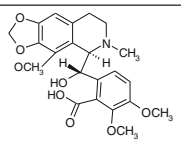	56.0×10^{-6}	34	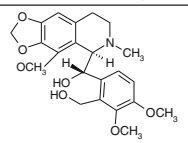	52.8×10^{-6}
35	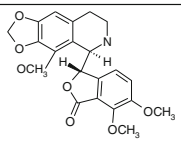	37.4×10^{-6}	36	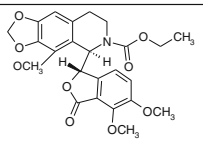	43.3×10^{-6}

against the CEM cell line, compounds were divided into active (10 molecules with $pIC_{50}>5.0$) and inactive (23 compounds with $pIC_{50}<4.5$) class compounds. PHASE (version 3.2, Schrodinger [28]) was used to generate CPHs. A maximum of 200 conformers were generated for each of the 36 noscapinoids by sampling the conformational space using a combined Monte-Carlo multiple minimum/low mode (MCMM/LMOD) method with OPLS-2005 force field, distance dependent dielectric solvation model, and a maximum of 1,000 iterations of post-minimization. Con-

formers not within 10 kcal mol^{-1} of the global minimum were discarded. Visual inspection and careful analysis of chemical features were conducted to guide the pharmacophore development process. Pharmacophore variants considered for anti-cancer activity were composed of seven sites with the following chemical features: hydrogen-bond acceptor (A, pink sphere), aromatic ring (R, ring), hydrophobic (H, green sphere), and positively charged group (P, blue sphere). Common pharmacophores were searched for in at least six of the ten active structures with a final box size of 1.0 $Å^3$, a tree depth of four and intersite distances of 2.0 Å. Several hypotheses were generated, of which the best (AAHHPRR) mapped onto compound **3**. Based on the PHASE scoring functions [15], this hypothesis was chosen as the final pharmacophore model for use in subsequent screening and QSAR investigations.

Assessment of significant CPH using partial least square analysis

The quality of CPHs was evaluated by developing atom-based 3D QSAR models [15] that correlate chemical structures with anti-cancer activity against the CEM cell line. The data set of 36 molecules was divided randomly into a training set of 26 and a test set of 10 molecules (Table 2) incorporating anti-cancer activity and chemical diversity. Atom-based QSAR models were built for the generated pharmacophores using a grid spacing of 1.0 Å to encompass the space occupied by the aligned training set molecules. Based on the occupation of a cube by a ligand atom of training set molecules, the total number of volume bits was assigned to a given cube. Thus, molecules were represented by a string of zeros and ones, according to the cubes they occupy and the different types of atoms/sites that reside in those cubes. QSAR models were generated by applying partial least squares (PLS) regression to the pool of binary-valued (as independent variables) and using pIC_{50} (as dependent variable) with three PLS factors. Each of these models was validated using a test set of ten molecules that were not considered during model generation.

Density functional theory calculations

The molecular structures of the noscapinoids obtained from the predictive pharmacophore model were used for density functional theory (DFT) calculations. The structures were energy minimized based on molecular mechanics (Macromodel, version 9.8, Schrodinger package [28]) during pharmacophore model development. However, in order to assess detailed aspects of the electronic structure of the molecules to calculate the various electronic properties accurately, we want the geometry of the molecule to be optimized at a specific level of theory. Thus, to ensure that the geometry of the structure is fairly reasonable, a complete geometric optimization of the structures is necessary. This is because small changes in the geometry can create very large changes in components of the electronic structure even if the overall self-consistent field (SCF) calculated energy (the total energy) of the structure does not change much. Therefore we carried out complete geometric optimization of the structure by applying hybrid DFT with B3LYP (Becke's three-parameter exchange potential and the Lee-Yang-Parr correlation functional) [29, 30], and using basis set 3-21 G* level [31–33] to calculate the electronic properties of noscapinoids at this level of theory. Similar computational methods have recently been used in calculating the electronic properties of molecules [34, 35]. Various electronic properties: 3D-MESP, dipole moment, LUMO, HOMO, and aqueous solvation energy were calculated using Jaguar (version 7.7, Schrodinger [28]). The MESP $V(r)$ at point r, due to a molecular system with nuclear charges $\{Z_A\}$, located at $\{R_A\}$ and the electron density $\rho(r)$ were derived using the equation:

$$V(r) = \sum_{A=1}^{N} \frac{Z_A}{|r - R_A|} - \int \frac{\rho(r')d^3r'}{|r - r'|} \quad (1)$$

where N denotes the total number of nuclei in the molecule, and the two terms refer to the bare nuclear potential and the electronic contributions, respectively. The balance of these two terms gives the effective localization of electron-rich regions in the molecular system. Molecular frontier orbitals HOMO and LUMO as well as MESP of all optimized structures were visualized with Maestro (version 9.1, Schrodinger package [28]). The outlines of these MESP maps provide a measure of the overall size of the molecule and the color-coded surface gives the locations of negative and positive electrostatic potentials.

Results and discussion

Effects of noscapinoids on proliferation of cancer cells

The absolute anti-cancer activity (IC_{50} value) of noscapinoids against human lymphoblastoid cells (CEM) were measured by MTS assay. The negative log of IC_{50} value (expressed as pIC_{50}) is used as anti-cancer activity in evaluating the structure–activity relationships of noscapinoids quantitatively. Given a normal distribution (bell-shaped curve) of activity values of a set of compounds, the rule of thumb in developing fairly accurate QSAR models suggests that the difference between the highest and lowest biological activity of the compounds should be three to four

Table 2 Experimental and predicted activities for training and test set compounds based on 3D quantitative structure–activity relationship (QSAR) models along with their calculated electronic features. pIC_{50} −(log IC_{50}), E_{solv} solvation energy, *LUMO* lowest unoccupied molecular orbital, *HOMO* highest occupied molecular orbital, *HLG* HOMO−LUMO energy gap

Sl. no.	Experimental pIC_{50} (M)	Predicted pIC_{50} (M)	Residual	E_{solv} (kcal/mol)	HOMO (eV)	LUMO (eV)	HLG (eV)	QM dipole (Debye)
1	4.780	4.970	0.190	−51.82	−0.214	−0.037	−0.177	13.61
2	4.548	4.770	0.222	−43.60	−0.211	−0.015	−0.196	12.49
3[a]	5.921	5.400	0.521	−79.32	−0.229	−0.078	−0.151	13.38
4	4.345	4.455	0.110	−47.54	−0.212	−0.023	−0.189	12.20
5	5.721	5.664	0.057	−83.65	−0.225	−0.076	−0.149	13.45
6	5.553	5.320	0.233	−43.34	−0.211	−0.066	−0.176	12.15
7	5.638	5.440	0.198	−52.70	−0.219	−0.069	−0.150	13.77
8[a]	4.810	4.880	0.070	−47.91	−0.213	−0.019	−0.194	12.13
9[a]	5.585	5.680	0.095	−55.02	−0.207	−0.062	−0.145	13.07
10	5.585	5.770	0.185	−47.37	−0.204	−0.065	−0.139	11.88
11[a]	5.520	5.300	0.220	−54.40	−0.214	−0.057	−0.157	14.89
12	5.523	5.413	0.110	−49.69	−0.218	−0.059	−0.159	13.61
13	5.000	4.937	0.063	−57.14	−0.217	−0.088	−0.129	13.08
14	5.000	5.160	0.160	−51.48	−0.212	−0.086	−0.126	11.71
15	4.410	4.600	0.190	−50.96	−0.221	−0.044	−0.177	13.03
16	4.516	4.710	0.194	−43.84	−0.215	−0.042	−0.173	12.29
17	4.319	4.170	0.149	−14.65	−0.207	−0.045	−0.162	6.14
18[a]	4.345	4.230	0.115	−14.77	−0.207	−0.036	−0.171	6.55
19	4.355	4.184	0.171	−13.73	−0.207	−0.024	−0.183	5.99
20	4.392	4.211	0.181	−10.62	−0.207	−0.044	−0.163	5.86
21	4.378	4.260	0.118	−19.15	−0.209	−0.045	−0.164	5.98
22[a]	4.346	4.300	0.046	−18.31	−0.209	−0.025	−0.184	6.40
23[a]	4.333	4.300	0.033	−17.19	−0.208	−0.042	−0.166	5.67
24	4.353	4.240	0.113	−19.41	−0.209	−0.043	−0.166	5.81
25[a]	4.356	4.310	0.046	−16.20	−0.206	−0.048	−0.158	5.80
26	4.286	4.166	0.120	−27.55	−0.214	−0.035	−0.179	14.60
27	4.403	4.350	0.053	−39.51	−0.214	−0.046	−0.168	14.18
28[a]	4.371	4.550	0.179	−31.40	−0.216	−0.031	−0.185	14.01
29	4.387	4.250	0.137	−38.09	−0.215	−0.049	−0.166	14.23
30	4.374	4.221	0.153	−34.14	−0.221	−0.050	−0.171	14.48
31	4.450	4.211	0.239	−34.64	−0.220	−0.039	−0.181	14.24
32	4.271	4.330	0.059	−39.63	−0.211	−0.016	−0.195	10.59
33 [a]	4.252	4.410	0.158	−37.78	−0.205	−0.011	−0.194	5.48
34	4.277	4.400	0.123	−37.32	−0.211	−0.017	−0.194	10.49
35	4.427	4.348	0.079	−24.37	−0.214	−0.035	−0.179	12.81
36	4.364	4.184	0.180	−11.72	−0.207	−0.036	−0.171	3.59

[a] Compounds in the test set

orders of magnitude [36]. However, with the array of noscapinoids examined in this study, the distribution of activities values was skewed to the left as the majority of compounds (22 out of 36) have weaker activity (pIC_{50}<4.5 M). Given this asymmetric distribution of activity, the actual range of raw experimental IC_{50} data in our case is, in fact, quite impressive (ranging from 1.2 to 56 μM, Table 1) and can be reasonably used to assess the structure–activity relationship among noscapinoids. Noscapine derivatives **3**, **5–7**, and **9–14** have significantly better activities ($pIC_{50}\geq$ 5.0 M) than the other compounds. On the contrary, derivatives **17–36** (aryl substituted N-carbamoyl/N-thiocarbamoyl noscapine analogues) generally showed very weak or no activity.

Table 3 Summary of QSAR results for five best common pharmacophore hypotheses (CPHs) with survival scores and statistical parameters. *SD* Standard deviation of the regression, R^2 value of R^2 for the regression, *F-value* variance ratio, *P* probability value of significance, *RMSE* residual mean square error between experimental and predicted activities, Q^2 cross validated R^2 using leave one out cross validation technique for the predicted activities, *Pearson-R*, correlation between the predicted and experimental activity for the test set

	CPH1 (AAHHPRR)	CPH2 (AAHHPRR)	CPH3 (AHHHPRR)	CPH4 (AAHHPRR)	CPH5 (AHHHPRR)
Survival score	13.489	13.466	13.464	13.412	13.405
Survival inactive	11.556	11.456	11.526	11.468	11.501
SD	0.250	0.268	0.260	0.257	0.254
R^2	0.912	0.882	0.795	0.799	0.804
F-value	31.400	26.300	28.400	29.200	30.000
P	3.97e-08	1.82e-07	9.58e-08	7.38e-08	5.86e-08
RMSE	0.215	0.258	0.251	0.322	0.262
Q^2	0.908	0.835	0.844	0.743	0.830
Pearson-*R*	0.951	0.938	0.953	0.899	0.931

Pharmacophore perception

The 36 noscapinoids considered as potential inhibitors of cell proliferation were divided randomly into an active set ($pIC_{50}>5.0$) comprised of 10 compounds (**3**, **5**–**7**, **9**–**14**) and an inactive set ($pIC_{50}<4.5$) comprised of 23 compounds (**4**, **15**, **17**–**36**); the remaining 3 compounds (**2**, **6**, **8**) were not classified in these categories and are termed the "intermediate" class. To determine the molecular components required for anti-cancer activity of noscapinoids, we generated various pharmacophore hypotheses containing five, six and seven sites using a terminal box size of 1.0 Å. Based on the molecular occupancy of the pharmacophore features, CPHs composed of five and six sites were rejected. A total of 1,838 CPHs consisting of seven sites belonging to 14 types (AAHHHPR, AAAAHPR, AAAHHHR, AAAAHRR, AAAAHHP, AAAHHHP, AAHHPRR, AAAHHPR, AAAHPRR, AAAHHRR, AAAAHHR, AAAAPRR, AHHHPRR and AAHHHRR) were subjected to stringent scoring function analysis with respect to active molecules and then with inactive molecules. Default parameters for site, vector, and volume were used for scoring CPHs. In addition, ligand activity (expressed as pIC_{50}) was incorporated with a weight of 1.0. The hypotheses that survived the scoring process were examined further by developing atom-based 3D-QSAR models. Table 3 summarizes the statistical data of the top ranked CPHs (with their survival scores) labeled as CPH1–CPH5. Among these, CPH1 was found to be the best based on different statistical parameters such as R^2, Q^2, Pearson-*R*, SD, RMSE and *F*-value. For example, R^2 and Q^2 values of 0.912 and 0.908 corroborate with the criteria for a QSAR model to be highly predictive. This yielded a good Pearson-*R* value of 0.951 and high *F*-value of 31.40. The root mean square error for the model was 0.215, which is an indicator of the quality of fit between the experimental and predicted

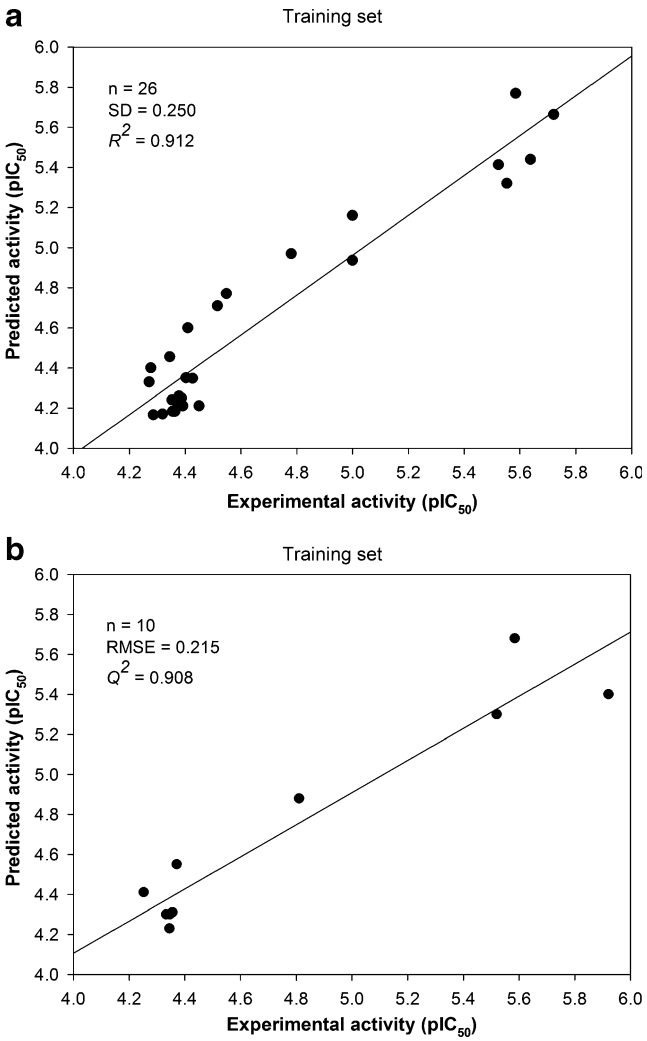

Fig. 2 Relationship between experimental and predicted activities (pIC_{50}) of **a** training set and **b** test set compounds based on 3D quantitative structure–activity relationship (QSAR) model; R^2=0.920; Q^2=0.885 and Pearson-*R*=0.951

pIC_{50} values (Fig. 2). The predicted and the experimental values of the training and test set molecules are given in Table 2. The most successful hypothesis—CPH1—was retained for further studies consisting of the following molecular components (Fig. 3):

1. Two acceptor features (A) mapping on the lone pair of vectors of oxygen atom (methoxy group) attached to dimethoxy isobenzofuranone ring (lower section of noscapine in Fig. 1).
2. Two aromatic ring features (R) mapping on the benzene rings.
3. Two hydrophobic group features (H) corresponding to two methyl groups
4. One positive group feature (P) corresponding to the nitrogen atom of the isoquinoline ring.

All highly active compounds of the noscapinoid family map all the functional features of the best predictive hypothesis (CPH1). For example, the two most potent

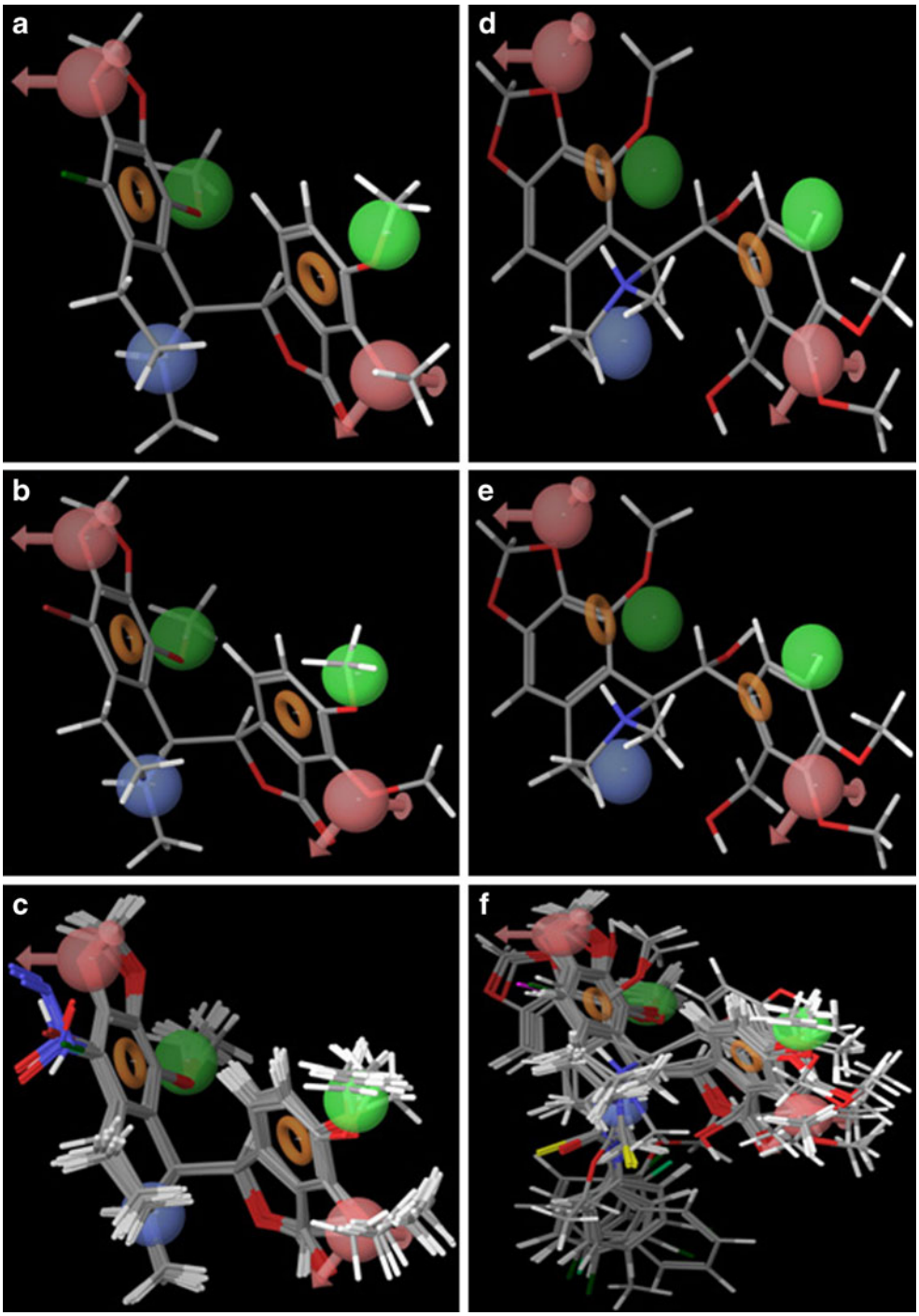

Fig. 3 Top ranked pharmacophore model (CPH1) mapped onto **a** the fittest compound **3**; **b** the most active compound **5**; **c** all the active compounds; on the inactive compounds **d 32**; **e 33** as well as **f** with all the inactive compounds. Pharmacophore variants considered for anticancer activity were composed of seven sites with the following chemical features: hydrogen-bond acceptor (A, *pink sphere*), aromatic ring (R, *ring*), hydrophobic (H, *green sphere*), and positively charged group (P, *blue sphere*)

members of the series—compounds **3** (9-chloro-noscapine) and **5** (9-bromo-noscapine)—map perfectly onto all the pharmacophoric features of hypothesis CPH1 (Fig. 3a,b). The other eight active compounds also map well onto the pharmacophore hypothesis (Fig. 3c). In contrast, the most inactive compounds **32** and **33** do not map onto the pharmacophore hypothesis (Fig. 3d,e), whereas some others map only partially (to only a few of the features of CPH1). The acceptor and polar groups seem to be crucial for anti-cancer activity, because these groups do not map in less active analogues. Also, in some of the less active analogues, the aromatic rings do not map properly, in spite of good mapping of the acceptor and positive group features (Fig. 3f). This stresses the equal importance of the aromatic rings in anti-cancer activity. Thus, overall, our complete pharmacophore model can distinguish accurately the active and inactive compounds of the noscapinoid family.

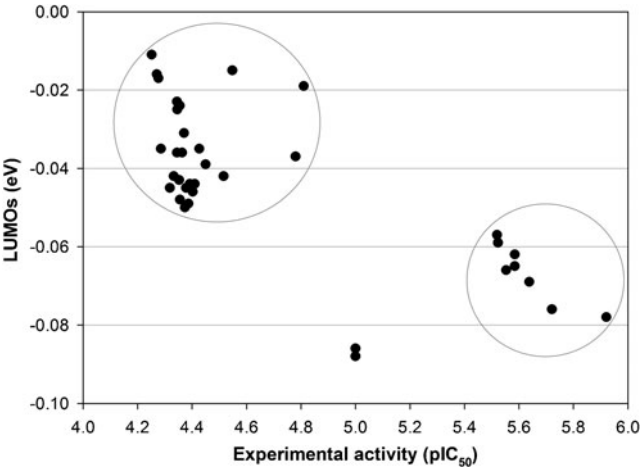

Fig. 4 Relationship between experimental activity (pIC_{50}) versus lowest unoccupied molecular orbital (LUMO)energy (eV) of the compounds. The active compounds (pIC_{50}>5.0) are clearly separated from the inactive compounds (pIC_{50}<4.5)

Lowest unoccupied and highest occupied molecular orbitals

Frontier orbital electron densities on molecules provide a useful means of characterizing donor–acceptor interactions in detail. It has been shown that these orbitals play a major role in governing many chemical reactions. For example, they are responsible for the formation of many charge transfer complexes. The energy of the HOMO is related directly to the ionization potential and it characterizes the susceptibility of the molecule towards an attack by electrophiles. On the other hand, the LUMO is related with electron affinity and gives an idea of the susceptibility of the molecule towards attack by nucleophiles. Among the noscapinoids used in this study, HOMO and LUMO energies are both small, ranging between −0.205 to −0.227 eV and −0.011 to −0.088 eV, respectively, indicating the fragile nature of the bound electrons (Table 2). The small energy gap between HOMO and LUMO energies (varies between 0.05 and 0.196 eV) makes both rapid electron transfer and exchange equally possible, making these compounds very reactive. Noscapinoids with higher anti-cancer activity (pIC_{50}>5.0) are those with more negative LUMOs values (on average, −0.071 eV) in comparison to the less active compounds (on average, −0.035 eV). Most active compounds can be distinguished clearly from less active compounds on the basis of their LUMO energies, as evident from the scatter plot of LUMO energies against activity (Fig. 4). Thus, manipulating the functional groups that affect LUMO energies could have a direct impact on the anti-cancer activity of noscapinoids. LUMO sites plotted onto the active molecules **1, 3, 5, 7, 11, 12** were scattered over the dimethoxy and the isobenzofuranone (lower section) ring; among compounds **9** and **10**, LUMO sites were located at the azido groups; whereas for compounds **13** and **14**, they are distributed over the nitro group, imply the susceptibility of these groups toward nucleophilic attack (Fig. 5). In contrast, among the least active noscapinoid compounds (**2**, **4**, **15**, **16**, **17–36**), such characteristic LUMO sites were missing. In striking contrast, HOMOs are located mainly at the isoquinoline ring in this series of noscapinoids.

Electrostatic potential profiles

Our results show that all the most active noscapinoids share specific electronic properties and are different from the least active compounds (Fig. 5). In our classification, all “most active compounds” showed an electronegative potential region (red color) near the oxygen atoms of the furanone ring, extending laterally over the oxygen atom of the dimethoxy group (L-shaped). Among the nitro derivatives (**13** and **14**), one more prominently localized negative charged region was seen near the oxygen atom of the nitro group. In the least active compounds, most negative potentials due to the oxygen atoms are missing. It is apparent from these results that the negative potentials near the oxygen atom of the dimethoxy isobenzofuranone ring and nitro group are crucial for activity. These electrostatic potential (ESP) profiles generated above are consistent with the pharmacophore model in which the hydrogen bond acceptor site is located at the oxygen atom of the methoxy isobenzofuranone ring.

Dipole moment

Dipole moments of the noscapinoids varied from 5.48 to 14.89 Debye (Table 2). All the most active compounds had higher dipole moment (> 11 Debye). However, some of the

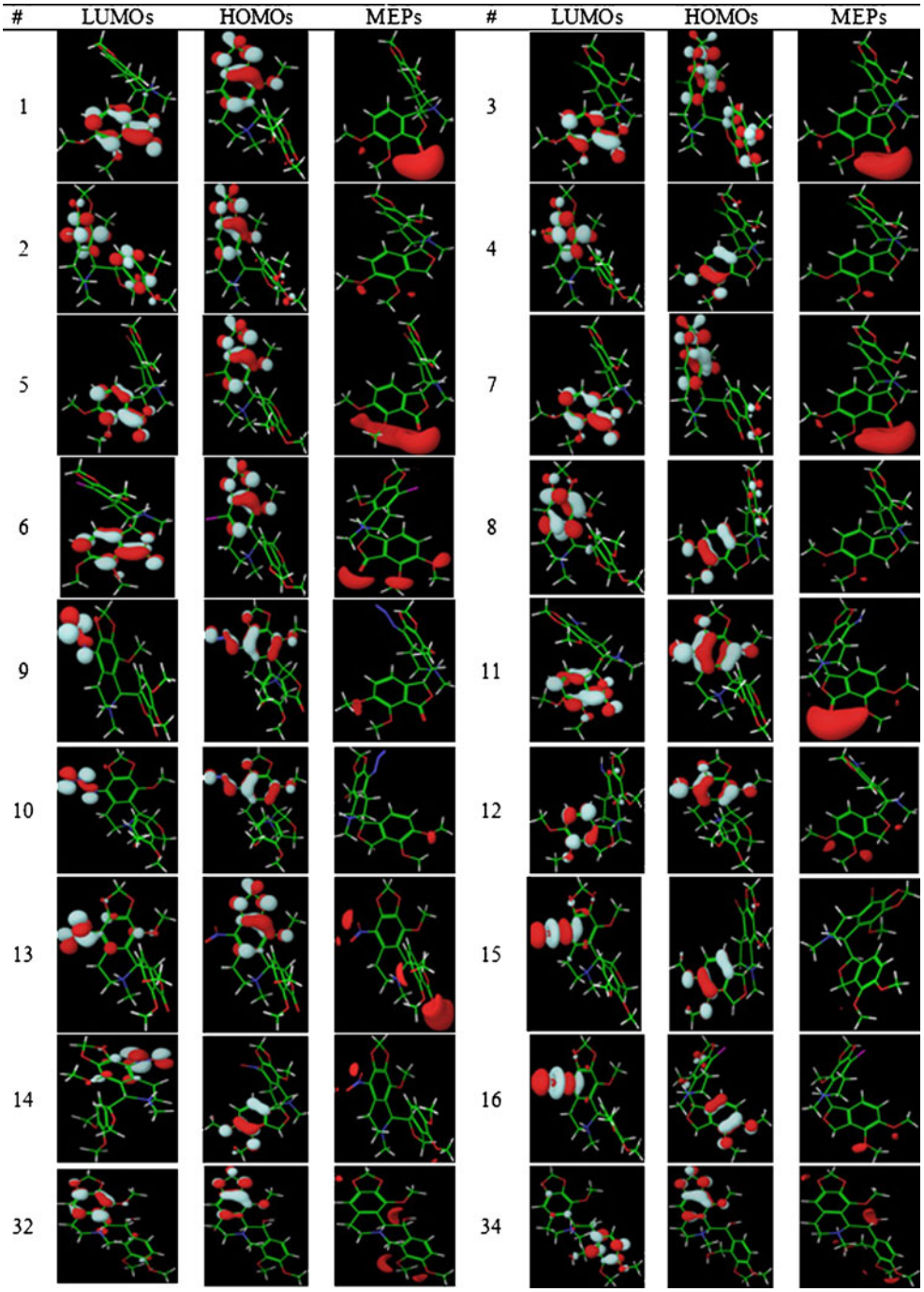

Fig. 5 Three dimensional LUMOs, highest occupied molecular orbitals (HOMOs) and electrostatic potential profiles of the optimized structures for most active (**3**, **5**–**7**, **9**–**14**), intermediate (**1**, **2**, **8**, **16**) and inactive (**4**, **15**, **32**, **34**) compounds. The orientations of the molecular structures are adjusted for better visualization of calculated molecular orbitals and electrostatic potential profiles

less active compounds also had high dipole moment values (for example, compounds **26**–**31** have a dipole moment of~ 14 Debye) and hence there is no clear correlation between dipole moment and biological activity.

Aqueous stabilization

Aqueous solubility is one of the most important properties contributing to the oral bioavailability of a drug. A value of 50 μg ml^{-1} is considered as the acceptable cut off for most preclinical drug development programs [37]. Solvation energy gives a measure of compound solubility, in that higher negative values of solvation free energy are indicative of higher aqueous solubility. In our noscapine derivative family, the solvation free energies of noscapinoids varied from −10.62 kcal mol^{-1} (**20**) to −83.63 kcal mol^{-1} (**5**) (Table 2) indicating the good aqueous solubility of these com-

pounds. The most active compounds have solvation energy > −50 kcal mol^{-1}, whereas inactive molecules—mostly aryl derivatives (**17**–**36**)—have less negative solvation energy (< −40 kcal mol^{-1}). Although, we did not pursue quantitative studies on the water solubility of noscapinoids, we routinely prepared stock solutions in ethanol or dimethylsulfoxide that were then diluted 100 to 1,000 fold in aqueous solution to determine the biological activity of noscapinoids. Furthermore, in our previous studies, these compounds were administered by feeding noscapine orally in aqueous solutions, or even by simply dissolving in drinking water [38]. Satisfactorily, these compounds also demonstrated favorable pharmacokinetics (clearance in 6–10 h) [39], consistent with the general belief that water-soluble drugs also display good pharmacokinetic behavior. Hence, the solvation energies computed in this study can be used to guide pharmacokinetic optimization of the compounds under study.

Conclusions

This body of work represents the first report of a highly predictive pharmacophore model of noscapine and its derivatives (the noscapinoids). A total of 1,838 different hypotheses were developed and examined. A final seven-point pharmacophore with the common features of a two hydrogen bond acceptor, two aromatics rings, two hydrophobic groups, and a positively charged group was associated with the most significant QSAR model. Calculated quantum chemical properties provide additional mechanistic details about the activity of these compounds. This work revealed that the presence of most negative potential regions above the oxygen atoms of the dimethoxy isobenzofuranone ring and the nitro group are essential for potent anticancer activity. The most active compounds are associated with higher negative values of LUMO energies. Aqueous solvation energies values give an indication of the aqueous solubility and can be used as a guide to pharmacokinetic optimization of these molecules. Modification of electronic properties in accordance with the results of this work by incorporating such structural features into the scaffold structure of noscapine will certainly achieve the final goal of improved anti-cancer noscapinoids.

Acknowledgments We thank Dr. William Beck for providing the drug-resistant CEM cell line used in this study and for advice. We are indebted to the anonymous reviewers of this manuscript for helpful suggestions. Grant support: National Institutes of Health (National Institute of Cancer) grants CA-095317-01A2 (H.C.J.) and Better Opportunities for Young Scientists in Chosen Areas of Science and Technology fellowship (SR/BY/L-37/09; Department of Science and Technology, Government of India) to P.K.N.

References

1. Chopra RN, Mukherjee BI, Dikshit BB (1930) Narcotine: its pharmacological action and therapeutic uses. Indian J Med Res 18:35–49
2. Winter CA, Flataker L (1954) Antitussive compounds testing methods and results. J Pharmacol Exp Ther 112:99–108
3. Idanpaan-Heikkila JE, Jalonen K, Vartiainen A (1967) Evaluation of the antitussive effect of noscapine and codeine on citric acid cough in guines-pigs. Acta Pharmacol Toxicol 25:333–338
4. Ye K, Ke Y, Keshava N, Shanks J, Kapp JA, Tekmal RR, Petros J, Joshi HC (1998) Opium alkaloid noscapine is an antitumor agent that arrests metaphase and induce apoptosis in dividing cells. Proc Natl Acad Sci USA 95:1601–1606
5. Ye K, Zhou J, Landen JW, Bradbury EM, Joshi HC (2001) Sustained activation of p34(cdc2) is required for noscapine-induced apoptosis. J Biol Chem 276:46697–46700
6. Zhou J, Gupta K, Yao J, Ye K, Panda D, Giannakakou P, Joshi HC (2002) Paclitaxel-resistant human ovarian cancer cells undergo c-Jun Nh2-terminal kinase-mediated apoptosis in response to noscapine. J Biol Chem 277:39777–39785
7. Zhou J, Panda D, Landen JW, Wilson L, Joshi HC (2002) Minor alteration of microtubule dynamics causes loss of tension across kinetochore pairs and activates the spindle checkpoint. J Biol Chem 277:17200–17208
8. Zhou J, Gupta K, Aggarwal S, Aneja R, Chandra R, Panda D, Joshi HC (2003) Brominated derivatives of noscapine are potent microtubule-interfering agents that perturb mitosis and inhibit cell proliferation. Mol Pharmacol 63:799–807
9. Aneja R, Vangapandu SN, Lopus M, Chandra R, Panda D, Joshi HC (2006) Development of a novel nitro-derivative of noscapine fpr the potential treatment of drug-resistant ovarian cancer and T-cell lymphoma. Mol Pharmacol 69:1801–1809
10. Aneja R, Vangapandu SN, Lopus M, Viswesarappa VG, Dhiman N, Verma A, Chandra R, Panda D, Joshi HC (2006) Synthesis of microtubule-interfering halogenated noscapine analogs that perturb mitosis in cancer cells followed by cell death. Biochem Pharmacol 72(4):415–426
11. Aneja R, Vangapandu SN, Joshi HC (2006) Synthesis and biological evaluation of a cyclic ether fluorinated noscapine analog. Bioorg Med Chem 14:8352–8358
12. Zhou J, Liu M, Luthra R, Jones J, Aneja R, Chandra R, Tekmal RR, Joshi HC (2005) EM012, a microtubule-interfering agent, inhibits the progression of multidrug-resistant human ovarian cancer both in cultured cells and in athymic nude mice. Cancer Chemother Pharmacol 55:461–465
13. Aggarwal S, Ghosh NN, Aneja R, Joshi HC, Chandra R (2002) A convenient synthesis of aryl-substituted N-carbamoyl/N-thiocarbamoyl narcotine and related compounds. Helv Chim Acta 85:2458–2462
14. Dixon SL, Smondyrev AM, Rao SN (2006) PHASE: A novel approach to pharmacophore modeling and 3D database searching. Chem Biol Drug Des 67:370–372
15. Dixon SL, Smondyrev AM, Knoll EH, Rao SN, Shaw DE, Friesner R (2006) PHASE: A new engine for pharmacophore perception, 3D QSAR model development, and 3D database screening. 1. Methodology and preliminary results. J Comput Aided Mol Des 20:647–671
16. Narkhede SS, Degani MS (2007) Pharmacophore refinement and 3D-QSAR studies of histamine H3 antagonists. QSAR Comb Sci 26:744–753
17. Tawari NR, Bag S, Degani MS (2008) Pharmacophore mapping of a series of pyrrolopyrimidines, indolopyrimidines and their congeners as multidrug resistance-associated protein (MRP1) modulators. J Mol Model 14:911–921

18. Bag S, Tawari NR, Degani MS (2009) Insight into inhibitory activity of *Mycobacterial* dihydrofolate reductase inhibitors by in silico molecular modeling approaches. QSAR Comb Sci 28:296–311
19. Politzer P, Murray JS, Peralta-Inga Z (2001) Molecular surface electrostatic potentials in relation to noncovalent interactions in biological systems. Int J Quantum Chem 85:676–684
20. Politzer P, Murray JS, Concha MC (2002) The complementary roles of molecular surface electrostatic potentials and average local ionization energies with respect to electrophilic processes. Int J Quantum Chem 88:19–27
21. Gejji SP, Suresh CH, Babu K, Gadre SR (1999) Ab initio structure and vibrational frequencies of $(CF_3SO_2)_2N^-Li^+$ ion pairs. J Phys Chem 103:7474–7480
22. Bhattacharrjee AK, Karle JM (1998) Functional correlation of molecular electronic properties with potency of synthetic carbinolamines antimalarial agents. Bioorg Med Chem 6:1927–1933
23. Bhattacharrjee AK, Karle JM (1999) Stereoelectronic properties of antimalarial artemisinin analogues in relation to neurotoxicity. Chem Res Toxicol 12:422–428
24. Vijayalakshmi KP, Suresh CH (2008) Role of structural water molecule in HIV protease-inhibitor complexes: a QM/MM study. J Comput Chem 29:1840–1849
25. Tomasi J, Bonaccorsi R, Cammi R (1990) In: Maksic R (ed) Theoretical models of chemical bonding. Springer, Berlin, pp 230–268
26. Beck WT, Cirtain MC (1982) Continued expression of vinca alkaloid resistance by CCRF-CEM cells after treatment with tunicamycin or pronase. Cancer Res 42:184–189
27. Skehan P, Storeng R, Scudiero D, Monks A, McMahon J, Vistica D, Warren JT, Bokesch H, Kenney S, Boyd MR (1990) New colorimetric anti-cancer activity assay for anti-cancer-drug screening. J Natl Cancer Inst 82:1107–1112
28. Schrödinger, LLC Phase, Version 3.2. Schrödinger, LLC, New York, NY; http://www.schrodinger.com
29. Lee C, Yang W, Parr RG (1988) Development of the Colle-Salvetti correlation-energy formula into a functional of the electron density. Phys Rev B 37:785–789
30. Becke AD (1993) A new mixing of Hartree-Fock and local density-functional theories. J Chem Phys 98:1372–1377
31. Binkley JS, Pople JA, Hehre WJ (1980) Self-consistent molecular orbital methods. 21. Small split-valence basis sets for first-row elements. J Am Chem Soc 102:939–947
32. Gordon MS, Binkley JS, Pople JA, Pietro WJ, Hehre WJ (1982) Self-consistent molecular-orbital methods. 22. Small split-valence basis sets for second-row elements. J Am Chem Soc 104:2797–2803
33. Pietro WJ, Francl MM, Hehre WJ, Defrees DJ, Pople JA, Binkley JS (1982) Self-consistent molecular orbital methods. 24. Supplemented small split-valence basis sets for second-row elements. J Am Chem Soc 104:5039–5048
34. Rodrigues T, dos Santos DJVA, Moreira R, Guedes RC (2010) A quantum mechanical study of novel potential inhibitors of cytochrome bc_1 as antimalarial compounds. Int J Quantum Chem 111:1196–1207. doi:10.1002/qua.22741
35. Tawari NR, Degani MS (2009) Pharmacophore mapping and electronic feature analysis for a series of nitroaromatic compounds with antitubercular activity. J Comput Chem 31:739–751
36. Checchi PM, Nettles JH, Zhou J, Snyder JP, Joshi HC (2003) Microtubule-interacting drugs for cancer treatment. Trends Pharmacol Sci 24:361–365
37. Budha NR, Mehrotra N, Tangallapally R, Rakesh QJ, Daniels AJ, Lee RE, Meibohm B (2008) Pharmacokinetically-guided lead optimization of nitrofuranylamide anti-tuberculosis agents. AAPS J 10:157–165
38. Landen JW, Lang R, McMahon SJ, Rusan NM, Yvon AM, Adams AW, Sorcinelli MD, Campbell R, Bonaccorsi P, Ansel JC, Joshi HC (2002) Noscapine alters microtubule dynamics in living cells and inhibits the progression of melanoma. Cancer Res 62:4109–4114
39. Dahlstrom B, Mellstrand T, Lofdahl CD, Hohansson M (1982) Pharmacokinetic properties of noscapine. Eur J Clin Pharmacol 22:535–539